On structural studies and cation distribution of La added Zn-Ni-Mg-Cu spinel nano ferrite

M Satalkar[a], S N Kane[a,1]
[a]Magnetic Materials Laboratory, School of Physics, D. A. University, Khandwa road, Indore-452001, India

E-mail: kane_sn@yahoo.com

Abstract. $Zn_{0.75-x}Ni_xMg_{0.15}Cu_{0.1}La_{0.02}Fe_{1.98}O_4$ (x = 0.0, 0.15, 0.30, 0.60, 0.75) was synthesized by sol-gel auto-combustion technique. As-burnt samples were thermally annealed at 500°C for 3 hrs. The as-burnt and annealed powder were characterized by X-ray diffraction (XRD) technique. The lattice constant ($a_{exp.}$), unit cell volume (V) and hopping length at A and B (L_A and L_B) deceases with increase in Ni^{2+} content (x). Scherrer's grain diameter (D) for as-burnt and annealed samples respectively ranges between 13.26 - 22.20 nm and 23.61 - 30.93 nm. After annealing the specific surface area of the particles decreases which can be attributed to increase in the particle size. Annealing leads to variation in cation distribution at tetrahedral (A) and octahedral [B] site, which affects theoretical lattice parameter ($a_{th.}$), ionic radii of A-site (r_A) and B-site (r_B), oxygen positional parameter (u), tetrahedral and octahedral bond length (R_A, R_B), shared tetrahedral and octahedral edge (d_{AE}, d_{BE}) and Neel's magnetic moment (n_B^N). The bond angles θ_1, θ_2, θ_3, θ_4, θ_5 and the distance between the metal ions at tetrahedral/octahedral site and anion (p, q, r) gives information about the A-A, A-B, B-B magnetic interaction. For lower values of Ni content ($0.0 \leq x \leq 0.3$), effective bond length ($R_{eff.}$) increases with annealing and for higher Ni content ($0.30 < x \leq .75$) R_{eff} decreases.

1. Introduction

Nanocrystalline spinel ferrites are a class of magnetic materials which have been the most attractive area of the research since the last 5 decades due to its remarkable applications in magnetic switches, magnetic resonance imaging, drug delivery, magnetic ferro-fluids, magnetic bulk cores, high-density data storage, micro-wave absorbers, the high frequency and power devices especially for electromagnetic interference suppression (EMIS) [1, 2]. It is believed that the production of ferrites will increase year by year as their applications become more and more diverse. Spinel ferrites have many versatile structural and magnetic properties owing to its feasibility to make a huge number of solid solutions of different metal cations and a large compositional variability. As the crystal structure of spinel ferrite is face centered cubic (fcc) with anions (O^{2-}) linked with two sub-lattices namely tetrahedral (A) and octahedral [B] sites. Distribution of cations over A and B sites has a profound effect on the structural and magnetic properties of spinel ferrites. According to the distribution of cations, there are normal, inverse and mixed/disorder spinels structures, which depends on the type of ions occupying A and B sites. Occupation of A site entirely with a divalent transition metal ion produces normal spinel, while occupation of B site with a divalent transition metal ion produces inverse spinel structure. If divalent transition metal ions are present at both A and B sites, then the

structure is mixed or disordered. Thus, AB_2O_4 type of compounds with spinel structure show interesting structural, electrical and magnetic properties, which vary with the nature of the ions, their charge and site distribution among tetrahedral and octahedral sites

It is well known that the desired structural and magnetic properties of soft ferrites can be tailored by the addition of suitable divalent, trivalent or tetravalent cations in to the spinel lattice. Incorporation of small amount of rare earth metal ions into the spinel ferrites may lead to structural distortion due to their large ionic radius and to induce strain and significantly modify the micro structural, electrical and magnetic properties. The rare-earth ions commonly reside at octahedral sites and have limited solubility in the spinel lattice due to their large ionic radii. But, the precise value of their solubility in the spinel lattice is not well known [3, 4]. Many researchers have studied the influence of various rare earth doping atoms on the properties of Li–Ni, Ni–Zn, Mn–Zn, Mg–Cu, Cu–Zn ferrites, etc. [5-9] and observed that different rare-earth ions behave differently in spinel ferrite and yield different structural properties. The structural properties and cation distribution of the spinel ferrites are governed by the chemical composition and the method of preparation. Altering the chemical composition is achieved by doping spinel ferrites with different transition metals and rare earth (R) ions. Both the type of the dopant and its amount are critical in changing the cation distribution and consequently the properties of the doped spinel ferrite [10, 11]. In spinel ferrites the proper choice of rare earth cation in spinel ferrite has a large influence upon the magnetic anisotropy of the system making the spinel ferrite an excellent option in place of hexaferrites or garnets. Thus, from the application point of view, the properties of ferrite nanoparticles can be tuned by the inclusion of suitable rare earth ions. Therefore, the main aim of the present work is to study the structural properties and cation distribution of as-prepared and thermally treated La^{3+} added Zn-Ni-Mg-Cu ferrite prepared by sol-gel auto-combustion method.

2. Experiment details

The compositions with the general formula $Zn_{0.75-x}Ni_xMg_{0.15}Cu_{0.1}Fe_2O_4$ spinel ferrite powders with x = 0.00, 0.15, 0.30, 0.45, 0.60, 0.75 with 2% addition of La^{3+} were prepared by the sol–gel auto-combustion method. For the synthesis, stoichiometric amount of citrate–nitrate/acetate pre-cursors [Zinc Nitrate - $Zn(NO_3)_2.6H_2O$, Nickel Acetate – $Ni(CH_3COO)_2.4H_2O$, Magnesium Acetate – $(CH_3COO)_2.Mg.4H_2O$, Copper Nitrate - $Cu(NO_3)_2.3H_2O$, Lanthanum nitrate - $La(NO_3)_3.6H_2O$ and Ferric Nitrate - $Fe(NO_3)_3.9H_2O$] were mixed with citric acid as fuel. Metal salt to fuel ratio was taken as 1:1. All the pre-cursors were dissolved in de-ionized water. Ammonia was then slowly added to the solution to adjust the pH at 7. Then the solution was heated at 120 ^oC in air till the loose powder (fluffy) was formed called as 'dry gel or as-burnt powder' which was then annealed at 500^oC for 3 hrs.

The characterization of as-burnt and annealed powders were performed by powder X-ray diffraction (θ-2θ configuration) on a Bruker D8 advance diffractometer (equipped with a fast counting detector based on Silicon strip technology (Bruker LynxEye detector) using Cu-K_α radiation (wavelength 'λ' =0.1540562 nm). Experimental lattice parameter ($a_{exp.}$), unit cell volume (V), x-ray density (ρ_{XRD}), Scherrer's grain diameter (D), surface area (S) of the particles and hopping length at A (L_A) and B (L_B) site of the studied samples were calculated as described in [12-15].

Cation distribution of all the studied samples was estimated using x-ray diffraction intensities, which directly depend on the position of atoms in the spinel unit cell while the position of the x-ray diffraction peaks depend on the shape and size of the unit cell. In this work, the Bertaut method [16] is used to determine the cation distribution. This method selects a few pairs of reflections according to the expression: $\frac{I_{hkl}^{obs}}{I_{h'k'l'}^{obs}} = \frac{I_{hkl}^{cal}}{I_{h'k'l'}^{cal}}$. Where, I_{hkl}^{obs} and I_{hkl}^{cal} are the observed and calculated intensities for the reflection (hkl), respectively. The reflections (220), (400), (440) and (422) were used to calculate x-ray intensity as these reflections are sensitive to cation distribution among tetrahedral and octahedral sites of the spinel lattice. The calculated and observed intensity ratios were compared for several combinations of cations distribution at (A) and [B] sites as describe in [17]. The best cation

distribution among the tetrahedral and octahedral sites for which theoretical and experimental ratios agree clearly, is taken to be the correct one. With the help of obtained cation distribution ionic radii of A-site (r_A) and B-site (r_B), theoretical lattice parameter ($a_{th.}$), oxygen positional parameter (u), tetrahedral/octahedral bond length (R_A, R_B), shared tetrahedral/octahedral edge (d_{AE}, d_{BE}), interionic distances between cation and anion (M_e-O) (p, q, r), the bond angles (θ_1, θ_2, θ_3, θ_4, θ_5) and effective bond length ($R_{eff.}$) were calculated as described in [14, 18, 19]. The radius of the ions involved in the above calculation has been taken from that reported by Shannon [20].

3. Results and discussions

The x-ray diffraction (XRD) patterns of as-burnt and annealed $Zn_{0.75-x}Ni_xMg_{0.15}Cu_{0.1}La_{0.02}Fe_{1.98}O_4$ spinel ferrite powders with x = 0.00, 0.15, 0.30, 0.45, 0.60, 0.75 are presented in Fig. 1a and 1b respectively. The diffractograms of all the studied samples reveal the formation of cubic spinel structure. No diffraction lines attributed to the presence of impurities or metal oxides were observed. It is observed from the XRD patterns of annealed samples (fig. 1b) that the peak intensity of each reflection increases, which indicate the complete crystallization of the samples.

Table 1 depicts the experimental lattice parameter ($a_{exp.}$), unit cell volume (V), hopping length for A-site (L_A) and B-site (L_B), x-ray density (ρ_{XRD}), Scherrer's grain diameter (D) and specific surface area (S) with Ni content (x) of as-burnt and ann. 500°C/3hrs $Zn_{0.75-x}Ni_xMg_{0.15}Cu_{0.1}La_{0.02}Fe_{1.98}O_4$. The observed decrease in the $a_{exp.}$, V, L_A and L_B with increasing Ni content of La added spinel ferrite for as-burnt and annealed system is ascribed to the replacement of an ion with higher ionic radius (Zn^{2+}: 0.060 nm) by an ion with lower ionic radius (Ni^{2+}: 0.055 nm). The variation in the lattice constant is in accordance with Vegard's law [21], which suggests that in solid solution spinels within the miscibility range, a linear change in lattice constant with the concentration of the components is observed. It can be observed from table 1 that with annealing $a_{exp.}$, V, L_A and L_B decreases (except for x = 0.00) because of the change in reaction kinetics during the annealing process of $Zn_{0.75-x}Ni_xMg_{0.15}Cu_{0.1}La_{0.02}Fe_{1.98}O_4$ nanoparticles. The decrease in the values of above mentioned parameters can also be ascribed to nanosized particles and increase in their ligand field. The increase in $a_{exp.}$, V, L_A and L_B after annealing for the un doped sample can be explained using surface disorder in the nanoparticles. Nanoparticle's surface plays an important role in determining its physical properties due to large surface to volume ratio. The surface disorder in ferrite nanoparticles is due to the chemical bond frustration and oxygen

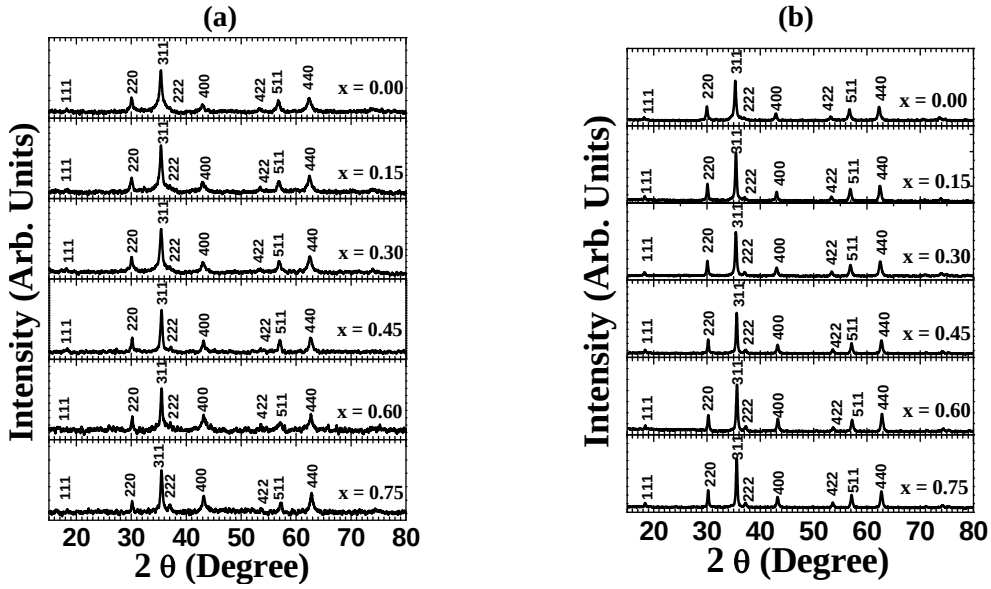

Figure 1 XRD pattern of (a) as-burnt, (b) annealed $Zn_{0.75-x}Ni_xMg_{0.15}Cu_{0.1}La_{0.02}Fe_{1.98}O_4$.

Table 1. Experimental lattice parameter ($a_{exp.}$), unit cell volume (V), hopping length for A-site (L_A) and B-site (L_B), x-ray density (ρ_{XRD}), Scherrer's grain diameter (D) and specific surface area (S) with Ni content (**x**) of as-burnt and annealed 500°C /3hrs $Zn_{0.75-x}Ni_xMg_{0.15}Cu_{0.1}La_{0.02}Fe_{1.98}O_4$ spinel ferrite.

x	$a_{exp.}$ (nm)	V (nm^3)	L_A (nm)	L_B (nm)	ρ_{xrd} (Kg/m^3)	D (nm)	S (m^2/g)
As-burnt							
0.00	0.8410	0.5948	0.3642	0.2973	5278.67	13.26	85.72
0.15	0.8403	0.5933	0.3639	0.2971	5269.50	16.61	68.55
0.30	0.8398	0.5923	0.3636	0.2969	5256.51	16.14	70.72
0.45	0.8381	0.5887	0.3629	0.2963	5266.02	21.36	53.34
0.60	0.8380	0.5885	0.3629	0.2963	5245.36	22.20	51.53
0.75	0.8378	0.5881	0.3628	0.2962	5226.55	21.66	53.00
(Ann. 500°C /3hrs)							
0.00	0.8426	0.5982	0.3649	0.2979	5248.65	23.61	48.42
0.15	0.8398	0.5923	0.3636	0.2969	5278.92	27.87	40.78
0.30	0.8400	0.5927	0.3637	0.2970	5252.76	26.00	43.93
0.45	0.8364	0.5851	0.3622	0.2957	5298.20	30.93	36.61
0.60	0.8354	0.5830	0.3617	0.2954	5294.48	27.96	40.53
0.75	0.8345	0.5811	0.3613	0.2950	5288.80	29.07	39.03

vacancies at different sub-lattices on the surface. With decreasing nanoparticle size, such surface disorder becomes more pronounced. The particle size for the un doped sample is the smallest among all the annealed particles. For annealed nanoparticles, the terminated surface unit cells get completed after getting atmospheric oxygen during the annealing process and reduce surface stresses/strains and hence, $a_{exp.}$, V, L_A and L_B increases. X-ray density (ρ_{xrd}) depends upon the molecular weight and on the lattice constant of the composition. ρ_{xrd} for as-burnt samples decreases with increase in Ni content (x). The decrease in x-ray density can be ascribed to the replacement of an ion (Zn) with higher mass by an ion (Ni) with lower mass. But non liner variation in the x-ray density is observed for annealed samples. ρ_{xrd} initially increases and then decreases for x = 0.30 and with further increase in Ni content ρ_{xrd} again increases for x = 0.45 and finally decrease for ($0.45 < x \leq 0.75$). Increase in the x-ray density can be attributed to the fact that the decrease in the volume of the unit cell overtakes the decrease in mass of the unit cell. And decrease in the x-ray density can be ascribable to the fact that the decrease in the mass of the unit cell overtakes the decrease in volume of the unit cell. With annealing ρ_{xrd} increases, (except for x = 0.0, 0.3) because during the sintering process, the thermal energy generates a force that drives the grain boundaries to grow over pores, thereby decreasing the pore volume and densifying the material. The specific surface area of the particles is the summation of the areas of the exposed surfaces of the particles per unit mass. Ferrites, offer new opportunities for enhancing the performances of solid catalysts [22] due to the much higher surface to bulk ratio compared to coarse micro-grained materials. High specific surface areas of particles are extremely important for heterogeneous catalytic processes. High surface area of ferrites is priority for catalytic purposes. There is an inverse relationship of particle size and density with surface area. In general, high surface areas imply small particle sizes. The smaller is the particle size, the larger is the surface area. Specific surface area of the as-burnt particles decreases with increasing in Ni content but the specific surface area of the annealed particles does not show any monotonic change with the doping content. After annealing the specific surface area of the particles decreases which can be attributed to increase in the particle size. Thus, as-burnt samples are more suitable for catalysts because of its high surface area. Non-monotonic behaviour of average crystallite size (D) with increasing Ni concentration is observed for both as-burnt and annealed systems. Such behaviour may be due to inhomogeneous stirring, diff gel/dry gel formation time etc. The crystal growth in the solution depends on various parameters

Table 2. Cation distribution (for A and B site), theoretical lattice parameter ($a_{th.}$) for as-burnt and annealed $Zn_{0.75-x}Ni_xMg_{0.15}Cu_{0.1}La_{0.02}Fe_{1.98}O_4$ system as a function of Ni content (x).

	A - site	**B - site**	**$a_{th.}$ (nm)**
	As-burnt		
0.00	$(Zn^{2+}_{0.70}Mg^{2+}_{0.075}Cu^{2+}_{0.05}Fe^{3+}_{0.175})$	$[Zn^{2+}_{0.05}Mg^{2+}_{0.075}Cu^{2+}_{0.05}La^{3+}_{0.02}Fe^{3+}_{1.805}]$	0.8425
0.15	$(Zn^{2+}_{0.60}Mg^{2+}_{0.10}Cu^{2+}_{0.05}Fe^{3+}_{0.25})$	$[Ni^{2+}_{0.15}Mg^{2+}_{0.05}Cu^{2+}_{0.05}La^{3+}_{0.02}Fe^{3+}_{1.73}]$	0.8404
0.30	$(Zn^{2+}_{0.45}Mg^{2+}_{0.10}Cu^{2+}_{0.05}Fe^{3+}_{0.40})$	$[Ni^{2+}_{0.30}Mg^{2+}_{0.05}Cu^{2+}_{0.10}La^{3+}_{0.02}Fe^{3+}_{1.58}]$	0.8388
0.45	$(Zn^{2+}_{0.30}Mg^{2+}_{0.10}Cu^{2+}_{0.05}Fe^{3+}_{0.55})$	$[Ni^{2+}_{0.45}Mg^{2+}_{0.05}Cu^{2+}_{0.10}La^{3+}_{0.02}Fe^{3+}_{1.43}]$	0.8372
0.60	$(Zn^{2+}_{0.10}Ni^{2+}_{0.30}Mg^{2+}_{0.10}Cu^{2+}_{0.05}Fe^{3+}_{0.45})$	$[Zn^{2+}_{0.05}Ni^{2+}_{0.30}Mg^{2+}_{0.05}Cu^{2+}_{0.05}La^{3+}_{0.02}Fe^{3+}_{1.53}]$	0.8363
0.75	$(Mg^{2+}_{0.10}Fe^{3+}_{0.90})$	$[Ni^{2+}_{0.75}Mg^{2+}_{0.05}Cu^{2+}_{0.10}La^{3+}_{0.02}Fe^{3+}_{1.08}]$	0.8363
	(Ann. 500^{o}C /3hrs)		
0.00	$(Zn^{2+}_{0.70}Mg^{2+}_{0.075}Cu^{2+}_{0.05}Fe^{3+}_{0.175})$	$[Zn^{2+}_{0.05}Mg^{2+}_{0.075}Cu^{2+}_{0.05}La^{3+}_{0.02}Fe^{3+}_{1.805}]$	0.8425
0.15	$(Zn^{2+}_{0.60}Ni^{2+}_{0.15}Cu^{2+}_{0.05}Fe^{3+}_{0.20})$	$[Mg^{2+}_{0.15}Cu^{2+}_{0.05}La^{3+}_{0.02}Fe^{3+}_{1.78}]$	0.8407
0.30	$(Zn^{2+}_{0.45}Ni^{2+}_{0.30}Mg^{2+}_{0.10}Cu^{2+}_{0.05}Fe^{3+}_{0.10})$	$[Mg^{2+}_{0.05}Cu^{2+}_{0.10}La^{3+}_{0.02}Fe^{3+}_{1.88}]$	0.8398
0.45	$(Mg^{2+}_{0.10}Cu^{2+}_{0.05}Fe^{3+}_{0.85})$	$[Zn^{2+}_{0.30}Ni^{2+}_{0.45}Mg^{2+}_{0.05}Cu^{2+}_{0.10}La^{3+}_{0.02}Fe^{3+}_{1.13}]$	0.8359
0.60	$(Zn^{2+}_{0.10}Mg^{2+}_{0.10}Cu^{2+}_{0.05}Fe^{3+}_{0.75})$	$[Zn^{2+}_{0.05}Ni^{2+}_{0.60}Mg^{2+}_{0.05}Cu^{2+}_{0.05}La^{3+}_{0.02}Fe^{3+}_{1.23}]$	0.8353
0.75	$(Mg^{2+}_{0.15}Fe^{3+}_{0.85})$	$[Ni^{2+}_{0.75}Cu^{2+}_{0.10}La^{3+}_{0.02}Fe^{3+}_{1.13}]$	0.8339

including extrinsic parameters (molecular concentration of the material, pH and temperature) and intrinsic parameters (heat of formation, site preferences, electronic configuration). Both the parameters can affect the growth process of the crystal. Increase in the average grain diameter for the synthesized samples with annealing temperature can be attributed to the crystal growth during annealing process. During thermal annealing, solid vapour surface of the crystals are replaced by solid - solid interface via diffusion to reduce the overall surface energy which leads to the expansion of volume. During annealing the activation energy essential for the nucleation is lowered which enhances the crystallite growth. At elevated temperature small grains begin to grow and the free energy of the system decreases as the energy of the grain boundaries is reduced.

Table 2 illustrates the cation distribution for tetrahedral (A) and octahedral [B] site. With increasing Ni content for as-burnt samples up to x = 0.45, Ni^{2+} ions occupy B site forcing Zn^{2+} ions to migrate completely from B to A site. For x = 0.60, 50% of Ni content occupies both A and B site and with further increase in Ni content i. e. for x = 0.75, Ni^{2+} ions migrate completely to B site. For x =0.75, Cu^{2+} ions occupy only B site. When Ni^{2+} ion is doped for Zn^{2+} ion, 66.7% Mg^{2+} ions occupy A site and 33.3% Mg^{2+} ions occupy B site. With annealing there is redistribution of cations from one site to another. With initial increase in Ni concentration (x = 0.15) for annealed samples, Ni^{2+} ions occupy A site forcing Mg^{2+} ions to migrate completely from A to B site. For x = 0.30, Ni^{2+} ions occupy A site and 66.7 % Mg^{2+} ions migrate to A site. 66.7 % Mg^{2+} ions occupy A site up to x = 0.60. But for x 0.75, Mg^{2+} ions occupy only A site. Ni^{2+} ions are distributed only on B site for $0.30 < x \leq 0.75$. No changes in the distribution of Cu^{2+} ions is observed for A and B site. But for x =0.75 Cu^{2+} ions occupy only B site. With increase in Ni content, Zn^{2+} ions occupy only A site up to x = 0.30 and for x = 0.45, Zn^{2+} ions migrate completely from A to B site. For x = 0.60, 66.7% Zn^{2+} ions occupy A site and the remaining Zn^{2+} ions occupy B site. The rare earth ion (La^{3+}) occupies only octahedral site for both as-burnt and annealed system. Perusal of table 1 shows that the cation distribution obtained from the x-ray diffraction is in close conformity with the real distribution, as there is realistic agreement between theoretical ($a_{th.}$) and experimental ($a_{exp.}$) lattice parameter (table 1).

A correlation between ionic radii of A-site (r_A), oxygen positional parameter or anion parameter (u), shared tetrahedral edge (d_{AE}) and tetrahedral bond length (R_A) has been established in table 3. The

Table 3. Ionic radii of tetrahedral/octahedral site (r_A, r_B), oxygen positional parameter (u), shared tetrahedral/octahedral edge (d_{AE}, d_{BE}) and tetrahedral/octahedral bond length (R_A, R_B) of as-burnt and annealed $Zn_{0.75-x}Ni_xMg_{0.15}Cu_{0.1}La_{0.02}Fe_{1.98}O_4$ system.

r_A (nm)	$u^{\bar{4}3m}$	d_{AE} (nm)	R_A (nm)	r_B (nm)	d_{BE} (nm)	R_B (nm)
As-Burnt						
0.0577	0.3843	0.3195	0.1956	0.0650	0.2752	0.2027
0.0568	0.3838	0.3180	0.1947	0.0647	0.2762	0.2029
0.0552	0.3828	0.3154	0.1932	0.0650	0.2784	0.2036
0.0535	0.3819	0.3127	0.1915	0.0654	0.2800	0.2039
0.0531	0.3817	0.3122	0.1912	0.0653	0.2804	0.2040
0.0498	0.3794	0.3066	0.1878	0.0672	0.2858	0.2058
(Ann. 500°C /3hrs)						
0.0577	0.3841	0.3196	0.1957	0.0650	0.2762	0.2033
0.0569	0.3840	0.3183	0.1949	0.0647	0.2755	0.2027
0.0570	0.3840	0.3184	0.1950	0.0644	0.2756	0.2027
0.0502	0.3799	0.3073	0.1882	0.0668	0.2841	0.2051
0.0513	0.3808	0.3091	0.1893	0.0660	0.2817	0.2041
0.0502	0.3802	0.3073	0.1882	0.0661	0.2828	0.2044

variation of u, d_{AE} and R_A has been studied as a function of ionic radii of A-site. It is observed from table 3 that with increase in r_A, for both as-burnt and annealed system u parameter, shared tetrahedral edge and tetrahedral bond length increases. As ionic radii of tetrahedral ions increases the tetrahedral site will expand in such a way that anions associated with tetrahedral site will move away from the tetrahedrally coordinated A-site cations, which results in the increase in u parameter, distance between unshared anions (d_{AE}) and the tetrahedral bond length (R_A). Similarly the correlation between ionic radii of B-site (r_B), oxygen positional parameter (u), shared octahedral edge (d_{BE}) and octahedral bond length (R_B) is also premeditated in table 3 for as-burnt and annealed La added Zn-Ni-Mg-Cu ferrite. The variation of oxygen positional parameter, shared octahedral edge and octahedral bond length has been studied as a function of ionic radii of B-site. As r_B increases d_{BE} and R_B increases but u parameter decreases. When r_B increases, the anions will move away from the octahedral site thus, increasing the distance between octahedral cation-anion (R_B) and the distance between the "shared anions (d_{BE}). Increase in r_B implies that the anions associated with B site will move towards tetrahedral site, resulting a decrease in the u parameter, as u is the value which represents the movement of tetrahedral oxygen. The tetrahedral bond length is smaller than octahedral bond length. The smaller values of R_A can be ascribed to a larger overlapping of orbitals of Fe^{3+} and O^{2-} at the A-site. There exists an inverse relationship between the covalent character of spinel and bond lengths. If the bond length increases/decreases with content of Ni, it can be concluded that there is a decrease/increase of iono-covalent character of the spinel with Ni content [23].

Magnetic information can also be extracted through structural data. Information about the magnetic interaction can also be obtained with the help of bond angles (θ_1, θ_2, θ_3, θ_4, θ_5) and the distance between the cation and anion (p, q, r). Figure 2 (a, b) illustrates respectively the variation of the bond angles θ_1, θ_2 and the distance between the cation and anion (q) with Ni content (x). The bond angles θ_1, θ_2 are the angles between A-O-B and q is the distance between the metal ions at tetrahedral site and anion. For all the studied samples, the bond angles θ_1, θ_2 increases and the distance between the metal ions at tetrahedral site and anion (q) decreases with Ni content, this suggests strengthening of A-B interaction. Figure 2 (c, d) respectively describes the variation of the bond angle between A-O-A (θ_5)

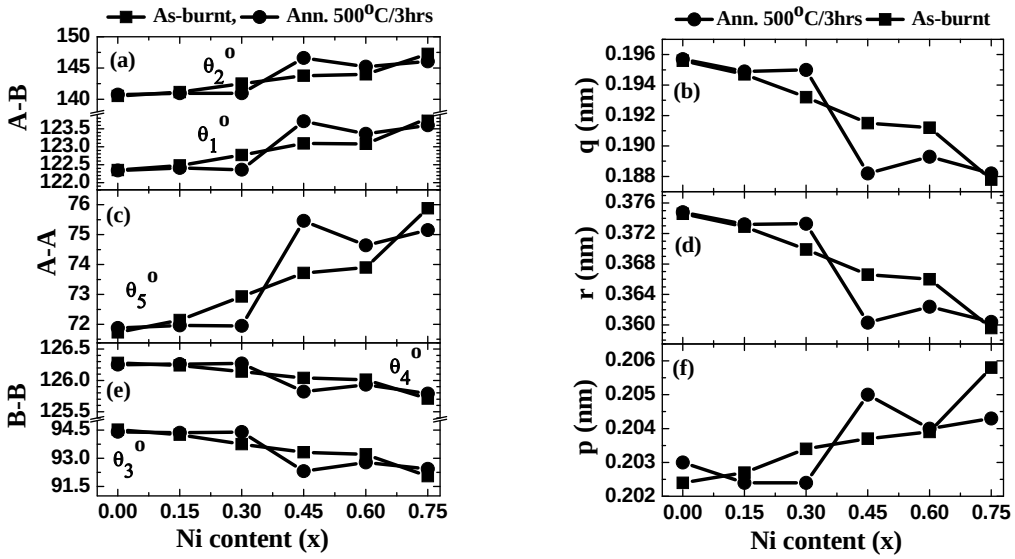

Figure 2. Variation of the bond angles **(a)** ($\theta_1^{A\text{-}O\text{-}B}$, $\theta_2^{A\text{-}O\text{-}B}$), **(c)** $\theta_5^{A\text{-}O\text{-}A}$, **(e)** ($\theta_3^{B\text{-}O\text{-}B}$, $\theta_4^{B\text{-}O\text{-}B}$) and the distance between cation and anion **(b)** q, **(d)** r, **(f)** p with Ni content (x) for as-burnt and annealed $Zn_{0.75-x}Ni_xMg_{0.15}Cu_{0.1}La_{0.02}Fe_{1.98}O_4$ system. Line connecting points are guide to the eye.

and the distance between the cation and anion (*r*) with Ni content (x). For as-burnt and annealed samples, θ_5, increases and *r* decreases with Ni content. Increase in the bond angles θ_5 and decrease in r suggests strengthening of A-A interaction. The variation of the bond angle between B-O-B (θ_3, θ_4) and the distance between the octahedral cation and anion (*p*) with Ni content is represented in fig. 2 (e, f) respectively. For as-burnt system θ_3, θ_4 decreases and the distance p increases with Ni content. But such linear trend is not observed in annealed samples. In annealed samples, the Ni content for which the bond angles between B-O-B decreases for the same value of x, *p* increases and for the value Ni content (x) for which θ_3, θ_4 increases for the same value of x, *p* decreases. Decrease in the bond angles θ_3, θ_4 and increase in p implies weakening of B-B interaction because the magnetic interaction between B-B is directly proportional to the bond angle θ_3, θ_4 and inversely proportional to *p*. And increase in the bond angles θ_3, θ_4 and decrease in p indicate strengthening of B-B interaction. The overall strength of the magnetic interactions (A−B and A−A) depends upon the bond length and bond angles between the cations and cation - anion. The strength is directly proportional to bond angle but inversely proportional to bond length. The same is proved in the figure 2. With annealing θ_1, θ_2, θ_5 decreases and θ_3, θ_4 increases except for x = 0.45, 0.60. This indicates weakening of A-B and A-A interaction and strengthening of the B-B interaction. And for x = 0.45 and 0.60, θ_1, θ_2, θ_5 increases and θ_3, θ_4 decreases with annealing indicating strengthening of A-B and A-A interaction and weakening of the B-B interaction. During annealing cations migrate from A site to B site or vice a verse and hence during migration of cations, interionic distances between cations and between cation and anion changes which bring variation in the bond angle between them.

The spinel ferrites with cubic crystal structure have two different crystallographic sub-lattices for magnetic ions, tetrahedral (A) and octahedral (B) sub-lattices. The magnetic order of the spinel ferrites mainly results from super-exchange interaction between the magnetic ions in the A and B sub-lattices mediated by oxygen ions. According to the Ne´el's two-sub-lattice model of ferrimagnetism, the magnetic moments of ions on the A and B sub-lattices are aligned antiparallel to each other and their spins have a collinear structure. Therefore, total magnetization is M_{oct} - M_{tet} (M_{oct} and M_{tet} are the sum of the magnetic moments on B sub-lattice and A sub-lattice, respectively) [24]. Néel magnetic moment

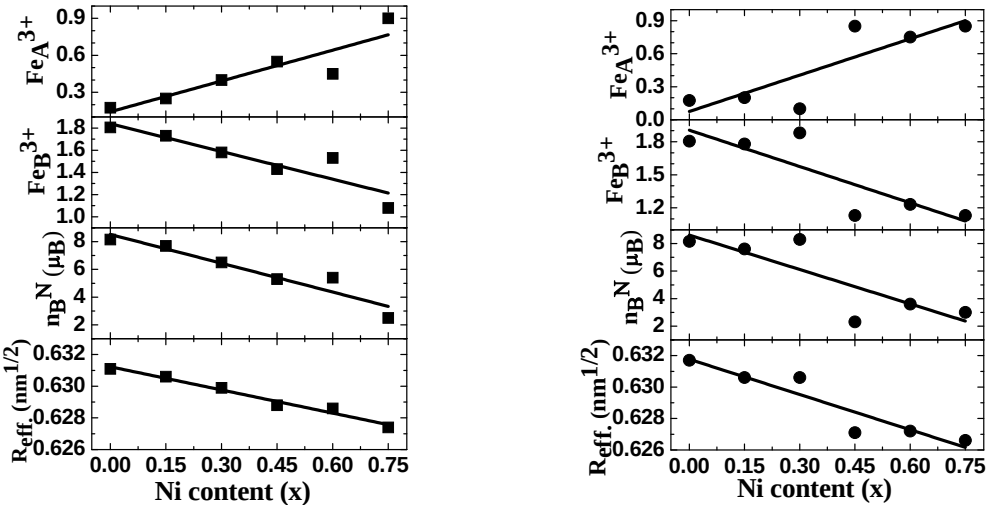

Figure 3. Variation of Fe^{3+} ions on A site (Fe_A^{3+}) and B site (Fe_B^{3+}), Néel magnetic moment (n_B^N) and effective bond length ($R_{eff.}$) with Ni content (x) for as-burnt (left panel) and annealed (right panel) $Zn_{0.75-x}Ni_xMg_{0.15}Cu_{0.1}La_{0.02}Fe_{1.98}O_4$ system. Line connecting points is linear fit to the experimental data.

(n_B^N) per formula unit in μ_B is calculated using the cation distribution (given in table 2) and and the ionic magnetic moments of Mg^{2+}, Ni^{2+}, Zn^{2+}, Cu^{2+}, La^{3+} and Fe^{3+} - $0\mu_B$, $2\mu_B$, $0\mu_B$, $1\mu_B$, $0\mu_B$ and $5\mu_B$ respectively. The variation of n_B^N with respect to Ni content is represented in fig. 3 for as-burnt (left panel) and annealed (right panel) La^{3+} added Zn-Ni-Mg-Cu spinel ferrite system. n_B^N decreases linearly with increase in Ni content because of increase in the concentration of Fe^{3+} ions on A site and decrease of Fe^{3+} ions on B site. The values of Fe^{3+} ions on A site (Fe_A^{3+}), B site (Fe_B^{3+}) and effective bond length ($R_{eff.}$) are shown in fig. 3 for as-burnt (left panel) and annealed (right panel) ferrite system. It can be clearly observed from fig.3 that Fe_A^{3+} increases and Fe_B^{3+} decreases linearly with Ni doping. With annealing there is redistribution of cations at tetrahedral (A) and octahedral (B) site, which changes the concentration of Fe^{3+} ions on A and B site and hence, n_B^N changes with annealing. The variation of the effective bond length ($R_{eff.}$) which is the distance between two cations, also affects the magnetic properties of a material. For the studied as-burnt and annealed samples $R_{eff.}$ decreases linearly with increase in Ni content. For lower values of Ni content ($0.0 \leq x \leq 0.3$) effective bond length increases with annealing and for higher Ni content ($0.30 < x \leq .75$) effective bond length decreases. Decrease in the effective bond length suggests decrease of the exchange coupling and increase in the effective bond length suggests increase of the exchange coupling.

4. Summary

Nanocrystalline Ni-substituted Zn-Mg-Cu-La ferrites were synthesized using sol-gel auto-combustion method. To study the thermal effect on the structural properties and cation distribution the as-burnt samples were annealed at 500^{o}C for 3hrs. X-ray diffraction patterns of as-burnt and annealed samples suggest the formation of single cubic spinel phase. Lattice constant ($a_{exp.}$), unit cell volume (V) and hopping length at A and B (L_A and L_B) of the studied samples decreases with increase in Ni content. Scherrer's grain diameter (D) for as-burnt and annealed samples respectively ranges between 13.26 - 22.20 nm and 23.61 - 30.93 nm. Relation between oxygen positional parameter (u), tetrahedral bond length (R_A), shared tetrahedral (d_{AE}) is interpreted by ionic radii of A-site and the relation between oxygen positional parameter (u), octahedral bond length (R_B) and shared octahedral edge (d_{BE}) have been deduced via ionic radii of B-site (r_B). Neel's magnetic moment (n_B^N) decreases linearly with increase in Ni content because of increase in the concentration of Fe^{3+} ions on A site and decrease of

Fe^{3+} ions on B site. With annealing θ_1, θ_2, θ_5 decreases and θ_3, θ_4 increases except for x = 0.45, 0.60. This suggests weakening of A-B and A-A interaction and strengthening of the B-B interaction.

Acknowledgments
Authors thank Dr. M. Gupta, UGC-DAE CSR, Indore India for performing XRD measurements. This work is supported by UGC-DAE CSR, Indore [CSR-IC/CRS-74/2014-15/2104].

References

[1] Pallai V and Shah D O 1996 *J. Magn. Magn. Mater.* **163** 243
[2] Skomski R 2003 *J. Phys. – Condens. Matter.* **15** R1
[3] Roy P K and Bera J 2007 *Mater. Res. Bull.* **42** 77
[4] Jiang J, Li L and Xu F 2007 *J. Rare Earths* **25** 79
[5] Al-Hilli M F, Li S and Kassim K S 2009 *Mater. Sci. Eng. B* **158** 1
[6] Costa A C F M, Diniz A P A, de Melo A G B, Kiminami R H G A, Cornejo D R, Costad A and Gama A L 2008 *J. Magn. Magn. Mater.* **320** 742
[7] Ravinder D and Vijaya Kumar K 2001 *Bull. Mater. Sc.* **24** 505
[8] Rezlescu N, Rezlescu E, Tudorache F and Popa P D 2004 *J. Optoelectr. Adv. Mater.* **6** 695
[9] Jiang J, Li L, Xu F and Xie Y 2007 *Mater. Sci. Eng. B* **137** 166
[10] Yehia M, Ismail S M and Hashhash A 2014 *J. Supercond. Nov. Magn.* **27** 771
[11] Hashhash A, Yehia M, Ismail S M and Ata-Allah S S 2014 *J. Supercond. Nov. Magn.* **27** 2305
[12] Cullity B D 1978 Elements of X-ray diffraction, second ed., Addison-Wesley Publishing Co.Philippines Ch. 10 p. 338
[13] Satalkar M, Kane S N, Ghosh A, Ghodke N, Barrera G, Celegato F, Coisson M, Tiberto P and Vinai F 2014 *J. Alloys Comp.* **615** S313
[14] Smit J and Wijn H P J 1959 Ferrites, Philips Technical Library, Eindhoven, The Netherlands, Ch. 8, p.144
[15] Qi X, Zhou J, Yue Z, Gui Z and Li L 2003 *Mater. Sci. Eng. B* **99** 278
[16] Weil L, Bertaut E F and Bochirol L 1950 *J. Phys. Radium* **11** 208
[17] Tanna R and Joshi H H 2013 *World Academy of Sc. And Eng. Tech.* **75** 78
[18] Lakhani V K, Pathak T K, Vasoya N H and Modi K B 2011 *Solid State Sc.* **13** 539
[19] Sickafus K E, Wills J M and Grimes N W 1999 *J. Am. Ceram. Soc.* **82** 3279
[20] Shannon R D 1976 *Acta Cryst.*, **A32** 751
[21] Vegard L 1969 *Zeitscchrift fur Physik*, **5** 17
[22] Hirabayashi D, Yosikawa T, Kawamoto Y, Mockizuki K and Sukuki K 2006 *Adv. in Sc. Tech.* 45 2169
[23] Levine B F 1973 *Phys. Rev.* **B7** 2591
[24] Néel L 1950 *C R Acad. Sci. Paris* **230** 375